

Semi-quantum approach to molecular dynamics simulation of thermal properties of low-dimensional nanostructures

A. V. Savin,^{1,*} Yuriy A. Kosevich,^{1,2,†} and Andres Cantarero^{2,‡}

¹*Semenov Institute of Chemical Physics, Russian Academy of Sciences, Moscow 119991, Russia*

²*Materials Science Institute, University of Valencia, PO Box 22085, ES46071 Valencia, Spain*

(Dated: June 3, 2019)

We present a detailed description of the semi-quantum approach to the molecular dynamics simulation of stochastic dynamics of a system of interacting particles. Within this approach, the dynamics of the system is described with the use of classical Newtonian equations of motion in which the quantum effects are introduced through random Langevin-like forces with a specific power spectral density (the color noise). The color noise describes the interaction of the molecular system with the thermostat. We apply this technique to the simulation of the thermal properties of different low-dimensional nanostructures. Within this approach, we simulate the specific heat and heat transport in carbon nanotubes, as well as the thermal transport in a molecular nanoribbon with rough edges and in a nanoribbon with a strongly anharmonic periodic interatomic potential. We show that the existence of rough edges and quantum statistics of phonons change drastically the thermal conductivity of the rough-edge nanoribbon in comparison with that of the nanoribbon with ideal (atomically smooth) edges and classical dynamics. We show how the combination of strong nonlinearity of the interatomic potentials with quantum statistics of phonons changes the low-temperature thermal conductivity of the nanoribbon with periodic interatomic potentials.

Molecular dynamics is a method of numerical modeling of molecular systems based on classical Newtonian mechanics. It does not allow for the description of pure quantum effects such as freezing out of high-frequency oscillations at low temperatures and the related decrease to zero of heat capacity for $T \rightarrow 0$. In classical molecular dynamics, each dynamical degree of freedom possesses the same energy $k_B T$, where k_B is Boltzmann constant. Therefore, in classical statistics the specific heat of a solid almost does not depend on temperature when only relatively small changes, caused by the anharmonicity of the potential, can be taken into account [1]. On the other hand, because of its complexity, a pure quantum-mechanical description does not allow in general the detailed modeling of the dynamics of many-body systems. To overcome these obstacles, different semiclassical methods, which allow to take into account quantum effects in the dynamics of molecular systems, have been proposed [2–8]. The most convenient for the numerical modeling is the use of the Langevin equations with color-noise random forces [5, 7]. In this approximation, the dynamics of the system is described with the use of classical Newtonian equations of motion, while the quantum effects are introduced through random Langevin-like forces with a specific power spectral density (color noise), which describe the interaction of the molecular system with the thermostat. Below we give a detailed description of this semi-quantum approach, in application to the simulation of specific heat and heat transport in different low-dimensional nanostructures.

The paper is organized as follows. In Sec. I we describe the temperature-dependent Langevin dynamics of the system under the action of random forces. If the random forces are delta-correlated in time domain, this corresponds to the white noise with a flat power spectral density. This situation corresponds to high enough temperatures, when $k_B T$ is larger than the quantum of the highest-frequency mode in the system, $k_B T \gg \hbar \omega_m$. But for low enough temperature, $k_B T \ll \hbar \omega_m$, the stochastic dynamics of the system should be described with the use of random Langevin-like forces with a non-flat power spectral density, which corresponds to the system with color noise. In Section II we describe the power spectra of the color noise, which is consistent with the quantum fluctuation-dissipation theorem [1, 9], and propose a method for color noise generation. In Secs. III and IV we apply the semi-quantum approach to the simulation of the specific heat and heat transport in carbon nanotubes. In Sec. V we use this method to the simulation of thermal transport in a molecular nanoribbon with rough edges. We show that the rough edges and quantum statistics of phonons change drastically the thermal conductivity of the rough-edge nanoribbon in comparison with that of the ribbon with ideal (atomically smooth) edges. In Sec. VI this technique is applied to the simulation of thermal transport in a nanoribbon with strongly anharmonic periodic interatomic potential. We show how the combination of strong nonlinearity of the interatomic potential with quantum statistics of phonons changes completely the behavior of the low-temperature thermal conductivity of the system.

*asavin@center.chph.ras.ru

†kosevich@polymer.chph.ras.ru, Yury.Kosevich@uv.es

‡Andres.Cantarero@uv.es

I. LANGEVIN EQUATIONS WITH COLOR NOISE

In the presence of a Langevin thermostat, equations of motion of coupled particles have the following form:

$$M_n \ddot{\mathbf{r}}_n = -\frac{\partial}{\partial \mathbf{r}_n} H - M_n \Gamma \dot{\mathbf{r}}_n + \Xi_n, \quad (1)$$

where the three-dimensional radius-vector $\mathbf{r}_n(t)$ gives the position of the n -th particle at the time instant t ($n = 1, 2, \dots, N$, N being the total number of particles), M_n is the particle mass, H is the Hamiltonian of the system and $\mathbf{F}_n = -\partial H / \partial \mathbf{r}_n$ gives the force applied to the n -th particle caused by the interaction with the other particles, $\Gamma = 1/t_r$ is the friction coefficient (t_r being the relaxation time due to the interaction with the thermostat), and $\Xi_n = \{\xi_{\alpha,n}\}_{\alpha=1}^3$ are random forces with the Gaussian distribution.

In the semi-quantum approach the random forces do not represent in general white noise. The power spectral density of the random forces in that description should be given by the quantum fluctuation-dissipation theorem [1, 9]:

$$\langle \xi_{\alpha n} \xi_{\beta m} \rangle_{\omega} = 2M_n \Gamma k_B T \delta_{\alpha\beta} \delta_{nm} p(\omega, T), \quad (2)$$

where $n, m = 1, 2, \dots, N$, $\alpha, \beta = 1, 2, 3$ are Cartesian components, δ_{nm} and $\delta_{\alpha\beta}$ are Kronecker delta-symbols. Here the positive and even in frequency ω function

$$\begin{aligned} p(\omega, T) &= \frac{1}{2} \frac{\hbar \omega}{k_B T} + \frac{\hbar \omega / k_B T}{\exp(\hbar \omega / k_B T) - 1} \\ &= \frac{\hbar \omega}{2k_B T} \coth(\hbar \omega / 2k_B T) \end{aligned} \quad (3)$$

gives the dimensionless power spectral density at temperature T of an oscillator with frequency ω . The first term in Eq. (3) gives the contribution of the zero-point oscillations to the power spectral density of random forces. With the use of Eqs. (2) and (3), we get the correlation function of the random forces as

$$\begin{aligned} \langle \xi_{\alpha n}(t) \xi_{\beta m}(0) \rangle &= \int_{-\infty}^{+\infty} \langle \xi_{\alpha n} \xi_{\beta m} \rangle_{\omega} e^{i\omega t} \frac{d\omega}{2\pi} \\ &= 2M_n \Gamma k_B T \delta_{\alpha\beta} \delta_{nm} \int_{-\infty}^{+\infty} p(\omega, T) e^{i\omega t} \frac{d\omega}{2\pi}. \end{aligned} \quad (4)$$

Let ω_m be the maximal vibrational eigenfrequency of the molecular system. At high temperatures, $T \gg \hbar \omega_m / k_B$, one has $p(\omega, T) = 1$ and the molecular system will perceive the random forces as a delta-correlated white noise:

$$\langle \xi_{\alpha n}(t) \xi_{\beta m}(0) \rangle = 2M_n \Gamma k_B T \delta_{\alpha\beta} \delta_{nm} \delta(t). \quad (5)$$

Therefore for high enough temperatures we deal with molecular dynamics with Langevin uncorrelated random forces. But for low temperatures, the random forces are

correlated according to the function given by Eqs. (3) and (4). In other words, for low temperatures the random forces in the system represent the color noise with the dimensionless power spectral density $p(\omega, T)$ given by Eq. (3).

II. COLOR NOISE GENERATION

For the implementation of the semi-quantum approach in molecular dynamics, random forces with the power spectral density given by $p(\bar{\omega})$ must be generated. Existing numerical techniques allow the generation of a random quantity from a prescribed correlation function [10]. This approximation was used in [7] in the modeling of thermodynamic properties of liquid ^4He above the λ point. But universal methods require in general the usage of high numerical resources. For instance, the utilization of the method proposed in [10] requires the execution of the Fast Fourier Transform for every random force value. We propose a technique which takes into account the specific form of the dimensionless power spectral density $p(\bar{\omega})$, where $\bar{\omega} = \hbar \omega / k_B T$ is a dimensionless frequency.

In terms of $\bar{\omega}$, the dimensionless power spectral density of random forces looks as

$$p(\bar{\omega}) = \frac{1}{2} \bar{\omega} + \frac{\bar{\omega}}{\exp(\bar{\omega}) - 1} = \frac{1}{2} \bar{\omega} \coth(\bar{\omega}/2). \quad (6)$$

The random force with dimensionless power spectral density, given by Eq. (6), can be presented as a sum of two independent functions, $p(\bar{\omega}) = p_0(\bar{\omega}) + p_1(\bar{\omega})$, where the first function, $p_0(\bar{\omega}) = \bar{\omega}/2$, has a linear power spectral density, while the second one is $p_1(\bar{\omega}) = \bar{\omega} / [\exp(\bar{\omega}) - 1]$.

To generate the color noise with a given dimensionless power spectral density $p(\bar{\omega})$, we will construct the dimensionless random vector functions $S_n(\tau) = \{S_{\alpha,n}\}_{\alpha=1}^3 = S_{0n}(\tau) + S_{1n}(\tau)$ of the dimensionless time $\tau = tk_B T / \hbar$, which will give the power spectral density of the random forces in Eqs. (1) as

$$\langle \xi_{\alpha n} \xi_{\beta m} \rangle_{\omega} = 2M_n \Gamma k_B T \langle S_{\alpha n} S_{\beta m} \rangle_{\bar{\omega}}, \quad (7)$$

such that

$$\begin{aligned} \langle \xi_{\alpha n}(t) \xi_{\beta m}(0) \rangle &= \int_{-\infty}^{+\infty} \langle \xi_{\alpha n} \xi_{\beta m} \rangle_{\omega} e^{i\omega t} \frac{d\omega}{2\pi} \\ &= 2M_n \Gamma k_B T \int_{-\infty}^{+\infty} \langle S_{\alpha n} S_{\beta m} \rangle_{\bar{\omega}} e^{i\omega t} \frac{d\omega}{2\pi} \\ &= \frac{2}{\hbar} M_n \Gamma (k_B T)^2 \int_{-\infty}^{+\infty} \langle S_{\alpha n} S_{\beta m} \rangle_{\bar{\omega}} e^{i\bar{\omega} \tau} \frac{d\bar{\omega}}{2\pi}, \end{aligned} \quad (8)$$

and

$$\langle S_{\alpha n} S_{\beta m} \rangle_{\bar{\omega}} = \langle S_{0\alpha n} S_{0\beta m} \rangle_{\bar{\omega}} + \langle S_{1\alpha n} S_{1\beta m} \rangle_{\bar{\omega}}. \quad (9)$$

Here, the uncorrelated random functions $S_{0n}(\tau)$ and $S_{1n}(\tau)$ will generate, in a *finite frequency interval*, the power spectra $p_0(\bar{\omega})$ and $p_1(\bar{\omega})$, respectively.

TABLE I: Value of the coefficients λ_i , c_i , $\bar{\Omega}_i$, $\bar{\Gamma}_i$.

coefficient	value	coefficient	value
$\lambda_1/\bar{\omega}_m$	1.763817	c_5	1.8315
$\lambda_2/\bar{\omega}_m$	0.394613	c_6	0.3429
$\lambda_3/\bar{\omega}_m$	0.103506	$\bar{\Omega}_5$	2.7189
$\lambda_4/\bar{\omega}_m$	0.015873	$\bar{\Omega}_6$	1.2223
$c_1/\bar{\omega}_m$	1.043576	$\bar{\Gamma}_5$	5.0142
$c_2/\bar{\omega}_m$	0.177222	$\bar{\Gamma}_6$	3.2974
$c_3/\bar{\omega}_m$	0.050319		
$c_4/\bar{\omega}_m$	0.010241		

For a molecular system with maximal vibrational eigenfrequency ω_m , we will construct the dimensionless random vector function $S_{0n}(\tau)$, whose power spectral density generates $p_0(\bar{\omega})$ in the frequency interval $[0, \bar{\omega}_m]$ ($\bar{\omega}_m = \hbar\omega_m/k_B T$). Each component of this vector can be written as a sum of dimensionless random functions

$$S_{0\alpha n}(\tau) = \sum_{i=1}^4 c_i [\eta_{\alpha n, i}(\tau) - \zeta_{\alpha n, i}(\tau)]. \quad (10)$$

The functions $\{\zeta_{\alpha n i}\}_{i=1}^4$ which generate the color noise, are the solutions of the linear equations:

$$\zeta'_{\alpha n i}(\tau) = \lambda_i [\eta_{\alpha n i}(\tau) - \zeta_{\alpha n i}(\tau)], \quad (11)$$

where $\zeta'_{\alpha n i}(\tau)$ is the derivative with respect to τ . Here $\eta_{\alpha n i}(\tau)$ are dimensionless white-noise random forces, with the correlation functions

$$\langle \eta_{\alpha n i}(\tau) \eta_{\beta k j}(0) \rangle = 2\delta_{\alpha\beta} \delta_{nk} \delta_{ij} \delta(\tau) / \lambda_i. \quad (12)$$

By solving Eqs. (11) in the frequency domain, $\zeta_{\alpha n i}$ can be substituted in Eq. (10) and the power spectra of S_{0n} can be obtained as

$$\langle S_{0\alpha n} S_{0\beta m} \rangle_{\bar{\omega}} = \delta_{\alpha\beta} \delta_{mn} \sum_{i=1}^4 \frac{2c_i^2 \bar{\omega}^2}{\lambda_i (\lambda_i^2 + \bar{\omega}^2)}. \quad (13)$$

The dimensionless parameters c_i and λ_i can be found by minimizing the integral

$$\int_0^1 \left[\frac{1}{2} x - \sum_{i=1}^4 \frac{2\bar{c}_i^2 x^2}{\bar{\lambda}_i (\bar{\lambda}_i^2 + x^2)} \right]^2 dx \quad (14)$$

with respect to the parameters $\bar{c}_1, \bar{\lambda}_1, \dots, \bar{c}_4, \bar{\lambda}_4$, where $\bar{c}_i = c_i/\bar{\omega}_m$, $\bar{\lambda}_i = \lambda_i/\bar{\omega}_m$. The coefficients c_i , λ_i , $i = 1, \dots, 4$, obtained within this procedure, are shown in Table I.

As one can see from Fig. 1, the function given by Eq. (13) approximates with high accuracy the linear function $p_0(\bar{\omega}) = \bar{\omega}/2$ in the frequency interval $0.015 \leq \bar{\omega}/\bar{\omega}_m < 1.1$.

On the other hand, the random function $S_{1\alpha n}(\tau)$, which will generate the power spectral density $p_1(\bar{\omega})$, can

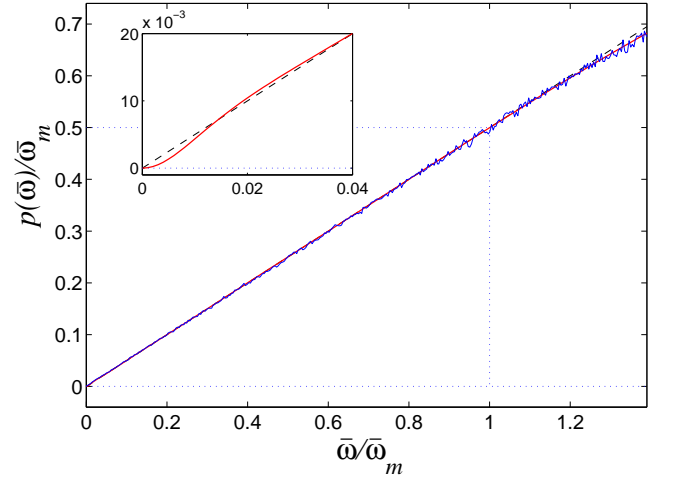


FIG. 1: Power spectral density of color noise $S_0(\tau)$ (blue line). Red line is given by Eq. (13), dashed line shows the linear function $p_0(\bar{\omega})/\bar{\omega}_m = \bar{\omega}/2\bar{\omega}_m$. The two lines practically coincide in the frequency interval $0.015 \leq \bar{\omega}/\bar{\omega}_m \leq 1.1$. The inset shows spectral densities given by Eq. (13) (red line) and by linear function $p_0(\bar{\omega})/\bar{\omega}_m$ (dashed line) in the frequency interval $0 \leq \bar{\omega}/\bar{\omega}_m \leq 0.04$. For color noise generation, Eqs. (11) were numerically integrated with the use of fourth order Runge-Kutta method with a constant integration step $\Delta\tau = 0.05/\bar{\omega}_m$.

be approximated by a sum of two random functions with relatively narrow frequency spectra:

$$S_{1\alpha n}(\tau) = c_5 \zeta_{\alpha n 5}(\tau) + c_6 \zeta_{\alpha n 6}(\tau). \quad (15)$$

In this sum the dimensionless random functions $\zeta_{\alpha n i}(\tau)$, $i = 5, 6$, satisfy the equations of motion as

$$\zeta''_{\alpha n i}(\tau) = \eta_{\alpha n i}(\tau) - \bar{\Omega}_i^2 \zeta_{\alpha n i}(\tau) - \bar{\Gamma}_i \zeta'_{\alpha n i}(\tau), \quad (16)$$

where, as before, $\eta_{\alpha n i}(\tau)$ are delta-correlated white noise functions:

$$\langle \eta_{\alpha n i}(\tau) \eta_{\beta k j}(0) \rangle = 2\bar{\Gamma}_i \delta_{\alpha\beta} \delta_{nk} \delta_{ij} \delta(\tau). \quad (17)$$

We can solve, as previously, Eq. (16) in the frequency domain and insert $\zeta_{\alpha n i}$ into Eq. (15) to obtain the power spectrum of $S_{1\alpha n}$:

$$\langle S_{1\alpha n} S_{1\beta m} \rangle_{\bar{\omega}} = \delta_{\alpha\beta} \delta_{mn} \sum_{i=5}^6 \frac{2c_i^2 \bar{\Gamma}_i}{(\bar{\Omega}_i^2 - \bar{\omega}^2)^2 + \bar{\omega}^2 \bar{\Gamma}_i^2} \quad (18)$$

The dimensionless parameters $\{c_i, \bar{\Omega}_i, \bar{\Gamma}_i\}_{i=5}^6$ can be found by minimizing the integral

$$\int_0^{40} \left[\frac{\bar{\omega}}{\exp(\bar{\omega}) - 1} - \sum_{i=5}^6 \frac{2c_i^2 \bar{\Gamma}_i}{(\bar{\Omega}_i^2 - \bar{\omega}^2)^2 + \bar{\omega}^2 \bar{\Gamma}_i^2} \right]^2 d\bar{\omega} \quad (19)$$

with respect to the parameters $c_5, \bar{\Gamma}_5, \bar{\Omega}_5, c_6, \bar{\Gamma}_6, \bar{\Omega}_6$. The obtained parameters are shown in Table I.

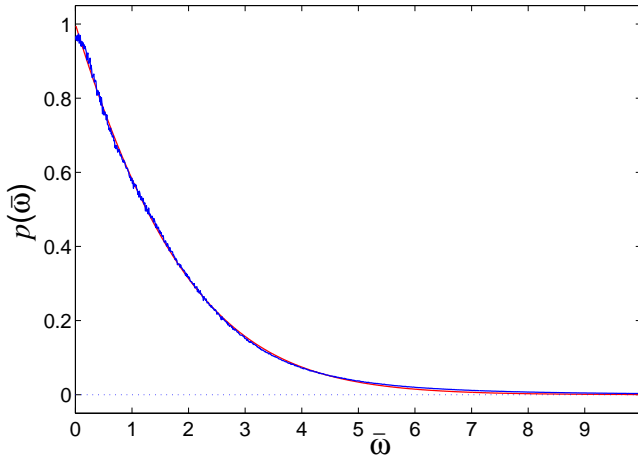


FIG. 2: Power spectral density of color noise $S_1(\tau)$, Eq. (18) (blue line). Red line shows the function $p_1(\bar{\omega}) = \bar{\omega}/[\exp(\bar{\omega}) - 1]$. For color noise generation, Eqs. (16) were numerically integrated with the use of fourth order Runge-Kutta method with a constant integration step $\Delta\tau = 0.02$.

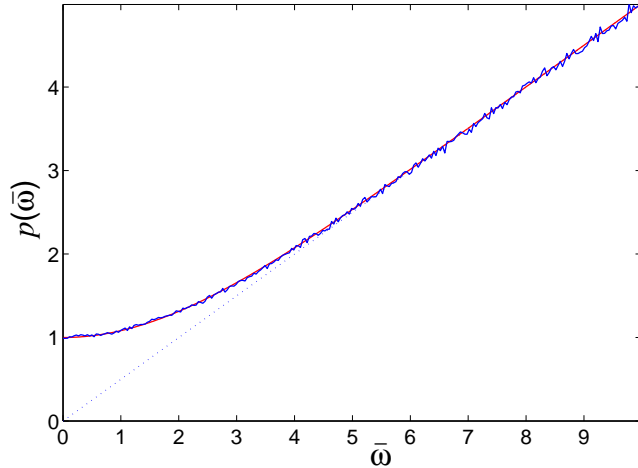


FIG. 3: Power spectral density of color noise $S_0(\tau) + S_1(\tau)$, given by the sum of Eqs. (13) and (18) (blue line). Red line shows the function $p(\bar{\omega}) = (\bar{\omega}/2) \coth(\bar{\omega}/2)$. For color noise generation, Eqs. (11) and (16) were numerically integrated with the use of fourth order Runge-Kutta method with a constant integration step $\Delta t = 0.005$. Maximal dimensionless frequency $\bar{\omega}_m = 10$.

As one can see from Fig. 2, the function, given by Eq. (18), approximates with high accuracy the function $p_1(\bar{\omega}) = \bar{\omega}/[\exp(\bar{\omega}) - 1]$ in the frequency interval $0 \leq \bar{\omega} \leq 10$.

Therefore in the semi-quantum approach one has to solve the Langevin equations (1) with random forces $\Xi_n = \{\xi_{\alpha n}\}_{\alpha=1}^3$, whose power spectral density is determined as:

$$\langle \xi_{\alpha n} \xi_{\beta m} \rangle_{\omega} = 2M_n \Gamma k_B T [\langle S_{0\alpha n} S_{0\beta m} \rangle_{\bar{\omega}} + \langle S_{1\alpha n} S_{1\beta m} \rangle_{\bar{\omega}}]$$

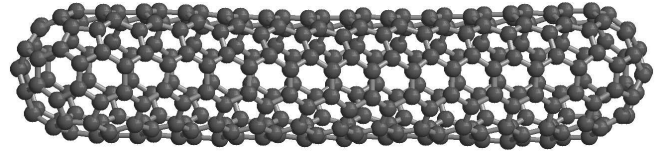


FIG. 4: Form of a single-walled carbon nanotube C_{300} with the zig-zag structure, which consists of $N = 300$ carbon atoms.

$$= 2M_n \Gamma k_B T \delta_{\alpha\beta} \delta_{mn} \left[\sum_{i=1}^4 \frac{2c_i^2 \bar{\omega}^2}{\lambda_i (\lambda_i^2 + \bar{\omega}^2)} + \sum_{i=5}^6 \frac{2c_i^2 \bar{\Gamma}_i}{(\bar{\Omega}_i^2 - \bar{\omega}^2)^2 + \bar{\omega}^2 \bar{\Gamma}_i^2} \right]. \quad (20)$$

From Eq. (8) we get the relation between the *dimension* $\xi_{\alpha n}(t)$ and *dimensionless* $S_{\alpha n}(\tau)$ random forces: $\xi_{\alpha n}(t) = \xi_{\alpha n}(\hbar\tau/k_B T) = k_B T \sqrt{2M_n \Gamma / \hbar} [S_{0\alpha n}(\tau) + S_{1\alpha n}(\tau)]$.

In Fig. 3 we show the comparison of the power spectral density for the dimensionless frequency $\bar{\omega}$, given by the sum of Eqs. (13) and (18), with the function $(\bar{\omega}/2) \coth(\bar{\omega}/2)$, Eq. (6). We see a very good coincidence in the frequency interval $[0, \bar{\omega}_m]$ for $\bar{\omega}_m = 10$.

To describe the dynamics of molecular system with an account for quantum statistics of molecular vibrations but without an account for zero-point oscillations, one has to keep only the last two terms, with $i = 5, 6$, in Eq. (20) and to solve numerically Eqs. (16) in order to simulate random forces in Eq. (1). Equations (16) play the role of low-frequency filter, which filters out the dimensionless high-frequency ("non-quantum") component of the white noise at low temperature.

It is worth mentioning in this connection that the considered semi-quantum approach permits one to obtain the correct value of the energy of zero-point oscillations. A semi-quantum account for zero-point oscillations in the modeling of the properties of liquid ${}^4\text{He}$ above the λ point has allowed to describe correctly the liquid state of the helium [7], while the classical molecular dynamics description (without an account for zero-point oscillations) predicts the solid state of the helium at the same low temperature.

III. TEMPERATURE DEPENDENCE OF SPECIFIC HEAT OF CARBON NANOTUBE

For the illustration of the implementation of the semi-quantum approach in molecular dynamics, in this Section we find the temperature dependence of specific heat of a single-walled carbon nanotube. We consider the nanotube with the (5,5) chirality index (the zig-zag structure), which consists of $N = 300$ carbon atoms, see Fig. 4. In the following we will use the molecular-dynamics model of the carbon nanotube, which was discussed in details in Ref. [11].

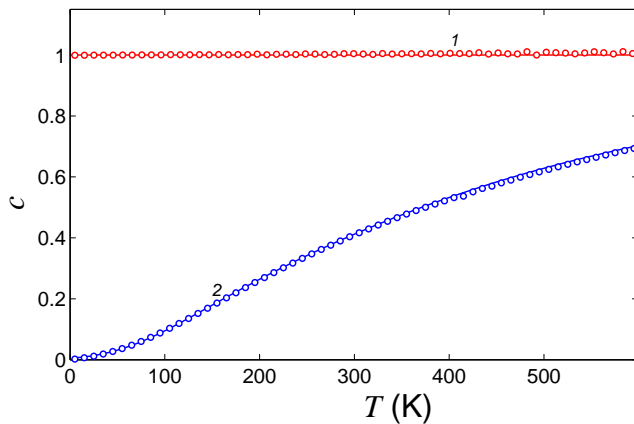


FIG. 5: Dependence of dimensionless specific heat $c = C/3Nk_B$ of a single-walled carbon nanotube C_{300} on temperature T . Line 1 shows the dependence obtained with classical Langevin thermostat, red circles give the result of numerical modeling, the straight line gives the value $c = 1$ ($C = 3Nk_B$). Line 2 gives the dependence obtained within the quantum description with the use of eigenmode spectra, blue circles give the result obtained within the semi-quantum approach.

To model nanotube dynamics at a temperature T in the classical approximation, we will solve the Langevin equation (1) with a white noise, where H is a Hamiltonian of the nanotube and all $M_n \equiv M$, M being a mass of a carbon atom. The correlation functions of the random forces Ξ_n , which describe the interaction of an n -th atom with the thermostat, are given by Eq. (5).

We take the initial conditions, which correspond to the ground stationary state of the nanotube, and integrate a system of equations of motion (1) for the time $t = 20t_r$, during which the system will reach the equilibrium state. The integration beyond this time will allow us to find the mean energy of the system $E(T) = \langle H \rangle$. Then the specific heat of the molecular system can be found from the temperature dependence of the mean energy $C(T) = dE(T)/dT$. As one can see from Fig. 5, the nanotube specific heat almost does not depend on temperature because the value of the mean energy is strictly proportional to temperature: $E(T) = 3Nk_B T$. This result shows both the correctness of the modeling and that the nanotube is a stiff structure which possesses weak anharmonicity of the dynamics of the constituting atoms.

To obtain power spectra of the thermal oscillations of the atoms in the carbon nanotube, one has to switch off the interaction with the thermostat after the establishment of thermal equilibrium in the system. In other words, one has to solve numerically the frictionless equations of motion, Eqs. (1) with $\Gamma = 0$ and $\Xi_n = \mathbf{0}$, with the initial conditions for \mathbf{r}_n and $\dot{\mathbf{r}}_n$, which correspond to the thermalized state of the molecular system. By performing the Fast Fourier Transform of the time-dependent particle velocities $\dot{\mathbf{r}}_n(t)$, one can get the power spectrum $p(\omega, T)$. To increase the accuracy of measurement, it is

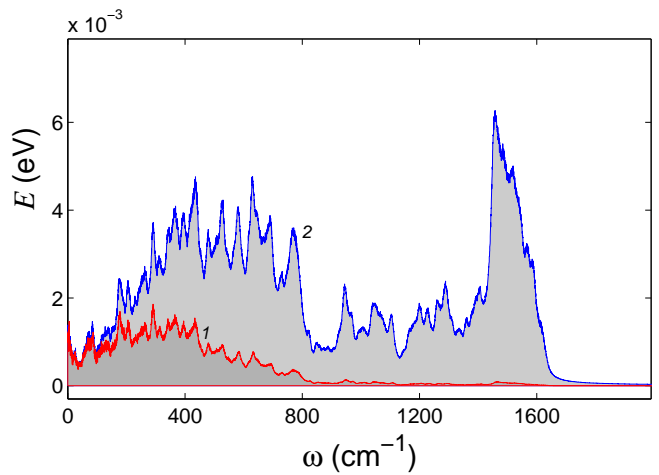


FIG. 6: Power spectral density of thermal vibrations of carbon nanotube C_{300} atoms at temperature $T = 300\text{K}$. Lines 1 and 2 give the densities obtained within the semi-quantum approach and classical description, respectively.

necessary to perform the averaging of the obtained results on different initial thermalized states of the system. Power spectral density of the thermal vibrations of the carbon nanotube atoms is shown in Fig. 6. As one can see from this figure, all vibrational modes are thermalized in the classical description.

Heat capacity of the quantum harmonic oscillator is given by the Einstein formula:

$$C(\Omega, T) = k_B \left(\frac{\hbar\Omega}{k_B T} \right)^2 \frac{\exp(\hbar\Omega/k_B T)}{[\exp(\hbar\Omega/k_B T) - 1]^2}, \quad (21)$$

where Ω is a frequency of the oscillator. This famous formula predicts that the heat capacity goes to zero for $T \rightarrow 0$. For low temperatures $T \ll T_E$, where $T_E = \hbar\Omega/k_B$ is the Einstein temperature, the vibrations of the quantum oscillator are partly frozen and its heat capacity $C \ll k_B$. For high temperatures $T \gg T_E$, the classical description is valid and $C \approx k_B$.

Carbon nanotube is a rigid structure in which the anharmonicity of atomic dynamics at room temperature is weakly pronounced: as one can see from line 2 in Fig. 6, the characteristic Debye temperature of the carbon nanotube is very high, $T_D \sim \hbar\omega_m/k_B \approx 2400\text{K}$, where $\omega_m \approx 1640 \text{ cm}^{-1}$ is the maximal phonon frequency in the system. Therefore we can obtain the temperature dependence of the carbon nanotube specific heat with the use of the spectrum of the harmonic (non-interacting) vibrational eigenmodes. To obtain the frequencies, we have to find all the eigenvalues of the square symmetric matrix $\partial^2 H / \partial \mathbf{r}_n \partial \mathbf{r}_m$ of the $3N \times 3N$ size: if λ is one of the eigenvalues, the eigenfrequency is determined as $\omega = \sqrt{\lambda/M}$. For $N = 300$ atoms in the nanotube, we have $3N = 900$ eigenmodes, from which the first 6 ones, which describe a rigid motion of the nanotube, have zero frequency, $\Omega_1 = \dots = \Omega_6 = 0$, while the other eigenfrequencies are nonzero and lie in the interval

$25.1 \text{ cm}^{-1} \leq \Omega_n \leq 1640.0 \text{ cm}^{-1}$, $n = 7, 8, \dots, 900$. We can obtain the temperature dependence of the nanotube specific heat with the use of Eq. (21):

$$C(T) = \sum_{n=7}^{3N} C(\Omega_n, T). \quad (22)$$

As one can see from Fig. 5, the nanotube specific heat monotonously goes to zero for $T \rightarrow 0$, and the quantum effects are essential for the carbon nanotube in the whole temperature range $T < 500\text{K}$, in which the specific heat per particle $C(T)$ is considerably less than the classical-statistics value $3Nk_B$.

To model the nanotube stochastic dynamics in the semi-quantum approach, we will use the Langevin equations of motion (1) with random forces $\Xi_n = \{\xi_{\alpha n}\}_{\alpha=1}^3$ with the power spectral density, given by $\langle \xi_{\alpha n} \xi_{\beta m} \rangle_{\omega} = 2M\Gamma k_B T \langle S_{1\alpha n} S_{1\beta m} \rangle_{\omega}$, see Eq. (20). Here it is explicitly taken into account that zero-point oscillations do not contribute to the specific heat of the system, and therefore one needs to account only for the random functions, given by Eq. (18).

Therefore the semi-quantum approach in this case amounts to the integration of Eqs. (1) and (16). From the value of the average energy of the system $E(T) = \langle H \rangle$, we can find the specific heat as $C(T) = dE(T)/dT$. As one can from Fig. 5, the temperature dependence of the carbon nanotube specific heat, obtained by studying the nanotube stochastic dynamics with color noise, coincides completely with the dependence, obtained from the spectrum of the harmonic vibrational eigenmodes in the system. Power spectral density of carbon atoms vibrations, see Fig. 6, shows that the semi-quantum approach describes the thermalization of only the low-frequency eigenmodes, with $\omega < \omega_T = k_B T / \hbar$. In such a way, the approach models the quantum freezing of the high-frequency eigenmodes at low temperature $T < T_D$. For the carbon nanotube, the classical description is definitely not valid at room temperature $T = 300\text{K}$, when the characteristic frequency $\omega_T = 208.5 \text{ cm}^{-1}$ is much less than the maximal one in the system, $\omega_m = 1640 \text{ cm}^{-1}$, see Fig. 6.

It is worth mentioning in this connection that the obtained results for the temperature dependence of the specific heat of the carbon nanotube C₃₀₀ almost do not depend on the relaxation time t_r . All the five values of t_r , $t_r = 0.1, 0.2, 0.4, 0.8, 1.6$ ps, give the same average energy $E(T)$ and specific heat $C(T)$ of the nanotube. One cannot use either too short t_r , when the system dynamics becomes the forced one, or too long t_r , which increases the computation time. We find that the optimal relaxation time for the carbon nanotube is $t_r = 0.4$ ps.

IV. MODELING OF THERMAL TRANSPORT IN CARBON NANOTUBE

The computation of the thermal conductivity can be performed by two methods. In the first method, the sys-

tem is thermalized with the use of equilibrium molecular dynamics and then the interaction with the thermostat is switched off. The current-current correlation function in the system is computed and the coefficient of thermal conductivity is found with the help of Green-Kubo formula based on this correlation function. In the second method, the method of non-equilibrium dynamics, the direct modeling of thermal transport is performed. For this purpose, two ends of the quasi-one-dimensional system are embedded in two thermostats with different temperatures. The stationary flux of energy is computed and the coefficient of thermal conductivity is determined from the known energy flux, temperature difference and length of the system. In the approach based on the non-equilibrium dynamics, the correct use of thermostats is important. The Langevin thermostat can be used in such approach.

The both methods model the thermal transport within the classical Newtonian dynamics and therefore do not allow to take into account the quantum effects. These methods can be justified only for high enough temperatures when the statistics of the system becomes completely classical. Nevertheless the method of the non-equilibrium dynamics can be easily adapted for the use in the semi-quantum approach to molecular dynamics modeling of thermal transport. Below we demonstrate this by example of a carbon nanotube.

For the classical modeling of thermal transport, we consider finite nanotube with chirality index (5,5) (see Fig. 4), and embed its left end in Langevin thermostat with temperature $T_+ = 1.1T$ and the right end in a thermostat with temperature $T_- = 0.9T$, where T is a temperature at which the thermal conductivity will be determined. For this purpose the dynamics of the atoms at the left/right end of the nanotube should be described by the Langevin equations (1) with a white noise with the correlation function given by Eq. (2) with temperature $T = T_+/T_-$. Dynamics of the atoms in the central part of the nanotube we describe with the Hamilton equations

$$M_n \ddot{\mathbf{r}}_n = -\partial H / \partial \mathbf{r}_n. \quad (23)$$

This allows us to find the distribution of temperature $T(x)$ and energy flux $J(x)$ along the nanotube, see Fig. 7. The detailed calculation of these quantities can be found in Ref. [11].

As one can see in Fig. 7, the constant energy flux and linear temperature gradient are established in the central part of the nanotube. This allows to determine the thermal conductivity of the nanotube of length L as

$$\kappa(L, T) = (L - 2L_e)J/[S(T_+ - T_-)], \quad (24)$$

where $L_e = 12.48 \text{ nm}$ is a length of nanotube ends embedded in thermostats, $S = \pi r^2$ is nanotube cross section (radius r is equal to 0.335 nm for the (5,5) single-walled nanotube).

For the semi-quantum modeling of thermal transport, we must use the Langevin equations (1) with the random forces $\xi_{\alpha n}$ with the power spectral density, given by

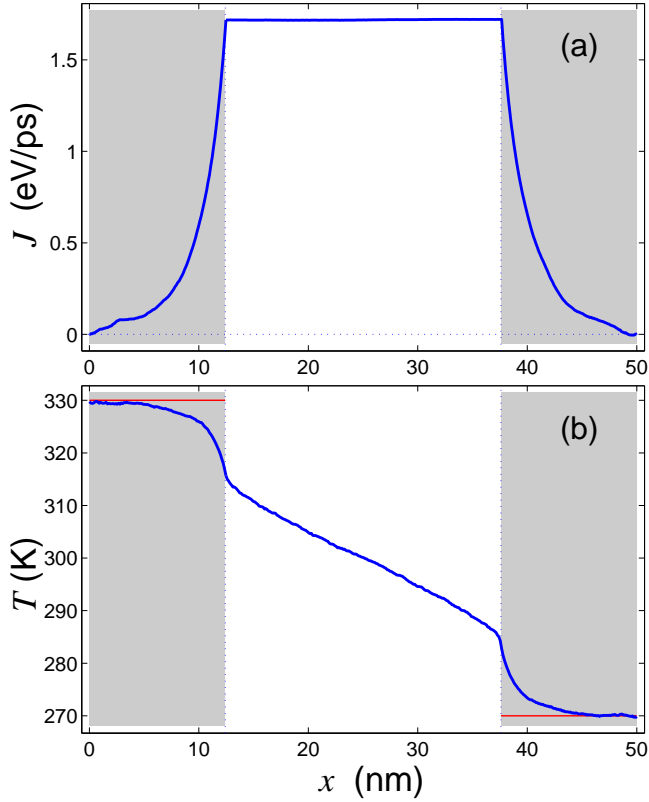


FIG. 7: Distribution of (a) local energy flux J and (b) local temperature T along the carbon nanotube (5,5) C_{4020} , x axis is along the nanotube axis. Nanotube length is $L = 50.08$ nm. Gray areas indicate the nanotube ends, embedded in Langevin thermostats with temperatures $T_+ = 330$ K and $T_- = 270$ K.

$\langle \xi_{\alpha n} \xi_{\beta m} \rangle_\omega = 2M\Gamma k_B T \langle S_{1\alpha n} S_{1\beta m} \rangle_\omega$, see Eq. (20), with temperature $T = T_+/T_-$. The color noise is determined as $\xi_{\alpha n}(t) = \xi_{\alpha n}(\hbar\tau/k_B T_\pm) = k_B T_\pm \sqrt{2M\Gamma/\hbar} S_{1\alpha n}(\tau)$. The zero-point oscillations do not contribute to the thermal transport, and therefore they will not be taken into account in the following and in all the formulas below we will put $S_{0\alpha n}(\tau) \equiv 0$. The thermal conductivity κ can be found with the use of Eq. (24).

We consider first the nanotube of the fixed length $L = 50.08$ nm (which corresponds to $N = 4020$ atoms). Temperature dependence of the nanotube thermal conductivity κ is shown in Fig. 8. As one can see from this figure, within the classical description the thermal conductivity κ_1 monotonously increases with the decrease of temperature. This property of "classical" thermal conductivity is related with the decrease of anharmonicity of lattice dynamics with the decrease of temperature, which in turn results in the increase of phonon mean free path. But the situation changes drastically with an account of quantum effects. In the semi-quantum description, thermal conductivity κ_2 first increases with the decrease of temperature from the high enough one but then it reaches its maximal value at $T = 350$ K and monotonously decreases to zero ($\kappa_2 \rightarrow 0$ for $T \rightarrow 0$). Such temperature

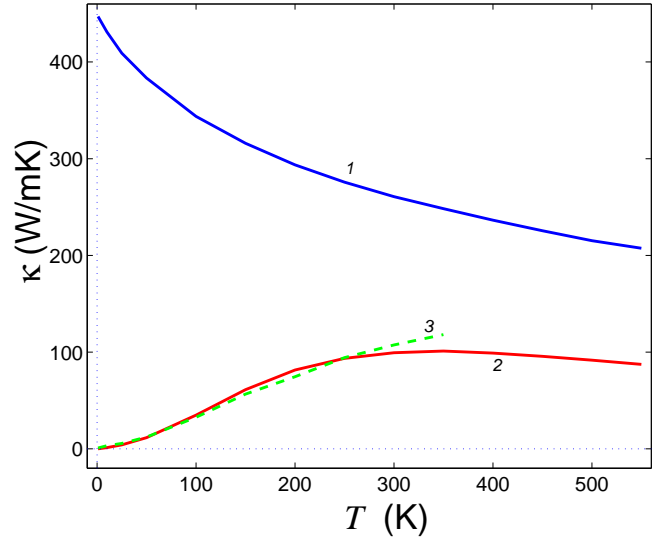


FIG. 8: Temperature dependence of thermal conductivity κ_i , ($i = 1, 2$), of the carbon nanotube (5,5) with length $L = 50.08$ nm: solid lines 1 and 2 are obtained within the classical and semi-quantum descriptions, respectively; dashed line 3 gives the temperature dependence $c(T)\kappa_1(T)$, where $c(T) = C(T)/3Nk_B$ is dimensionless specific heat of the carbon nanotube at temperature T .

dependence of thermal conductivity, which is characteristic for solids [12, 13], is related with the quantum decrease of the specific heat of the system. This is confirmed by the property that at low temperature $T \leq 250$ K the thermal conductivity of the nanotube in the semi-quantum approach $\kappa_2(T)$ is described with high accuracy by the relation $\kappa_2(T) \approx c(T)\kappa_1(T)$, where $c(T) = C(T)/3Nk_B$ is dimensionless specific heat of the carbon nanotube at temperature T , see Figs. 5 and 8.

Length dependence of the nanotube thermal conductivity is shown in Fig. 9. As one can see from this figure, both methods give monotonous increase of the thermal conductivity with the nanotube length. The semi-quantum description gives the lower value of the coefficient than the classical one for all the considered nanotube lengths. As one can see from this figure, line 2 lies below line 3 for relatively short nanotubes, which is consistent with Fig. 8. But at some nanotube length the line 2 intersects the line 3. This means that for longer nanotube lengths the mean free path of "semi-quantum" phonons is larger than that of purely classical phonons. This in turn is related with the decrease in general of phonon mean free path with phonon frequency and the property that the *mean frequency* of "semi-quantum" phonons is always lower than that of classical phonons. The intersection at some nanotube length of the line 2 with line 3 in Figs. 8 and 9 means that short enough nanotubes effectively filter out the high-frequency and short-mean-free-path phonons, as it occurs in mesoscopic one-dimensional samples, see, e.g., Ref. [14]. Line 2 should intersect the line 1 at even longer lengths, when ther-

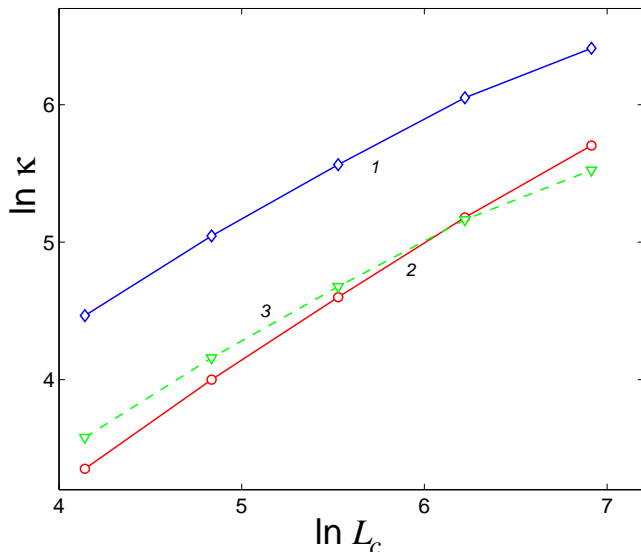


FIG. 9: Thermal conductivity κ versus length of the central part $L_c = L - 2L_e$ of the carbon nanotube (5,5) obtained with the use of classical (solid line 1) and semi-quantum (solid line 2) descriptions, and thermal conductivity $c(T)\kappa_1(T)$ (dashed line 3, as line 3 in Fig. 8) at $T = 300\text{K}$. The length L_c is measured in \AA , the thermal conductivity κ - in W/mK .

mal conductivity of the "semi-quantum" nanotube will become larger than that of purely "classical" nanotube. Figure 12 (b) below shows that similar situation can be also realized in a nanoribbon. Concerning carbon nanotubes, at $T = 300\text{K}$ such intersection can be realized only in very long nanotubes because of their very high Debye temperature (which in fact exceeds the melting temperature of the material).

V. THERMAL CONDUCTIVITY OF NANORIBBON WITH ROUGH EDGES

It was predicted analytically and confirmed by classical molecular dynamics simulations that rough edges of molecular nanoribbon (or nanowire) cause strong suppression of phonon thermal conductivity due to strong *momentum-nonconserving* phonon scattering [15, 16]. In the case of nonlinear interatomic potential, the ribbon has a finite, length-independent thermal conductivity, while in the case of harmonic interatomic potential, the thermal conductivity decreases with the ribbon length (and the ribbon behaves as a thermal insulator). Essentially for both interatomic potentials, the thermal conductivity increases with the length of the nanoribbon with ideal (atomically smooth) edges. In the case of harmonic interatomic potential, phonons in the nanoribbon with rough edges experience effective localization due to strong antiresonance multichannel reflection from side atomic oscillators in the rough edge layers (the Anderson-Fano-like localization due to interference ef-

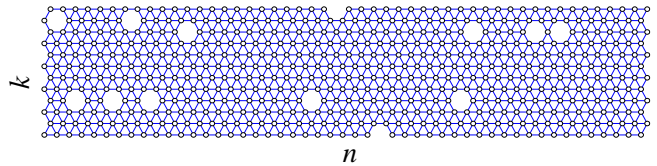


FIG. 10: Molecular ribbon made of $K = 12$ molecular chains. Density and widths of rough edges are $d = 0.95$ and $K_1 = 4$, respectively. Lines connect the interacting atoms.

fects in phonon backscattering, see [15, 16]). Apparently such strong backscattering can localize phonons with the wavelength shorter than the ribbon length. Within the classical description, such effect does not depend on temperature. But this picture will be changed if we take into account the quantum effects. The latter result in thermalization and correspondingly in participation in low temperature thermal transport of long wave phonons only. The long wave phonons are much less affected by surface roughness than the short wave phonons and therefore the effect of thermal conductivity suppression should decrease with the decrease of temperature. Below we demonstrate this effect within the proposed semi-quantum approach.

We consider the system which consists of K parallel molecular chains in one plane [16]. Let k be the chain number, n be the molecular number in the chain, then the equilibrium position of the n -th atom in the k -the chain will be $x_{k,n}^0 = na + [1 + (-1)^k]a/4$, $y_{k,n}^0 = bk$, where a and b are, respectively, the intra- and interchain spatial periods, see Fig. 10.

Only the longitudinal displacements are taken into account in a simplest scalar model of two-dimensional crystal: $x_{k,n}(t) = x_{k,n}^0 + au_{k,n}(t)$, $y_{k,n} \equiv y_{k,n}^0$, where $u_{k,n}$ is a dimensionless longitudinal displacement of the (k, n) -th molecule from its equilibrium position. Hamiltonian of the system has the form as

$$H = \sum_{k=1}^K \sum_{n=1}^N \frac{1}{2} M a^2 \dot{u}_{kn}^2 + E_0 \sum_{k=1}^K \sum_{n=1}^{N-1} V(u_{k,n+1} - u_{k,n}) + E_0 \sum_{k=1}^K E_k, \quad (25)$$

where N is a number of molecules in each chain, M is a mass of molecule, E_0 is a characteristic interaction energy, $V(\rho)$ is the dimensionless potential of the nearest-neighbor intrachain interactions, ρ describes relative displacements of the nearest-neighbor atoms, E_k describes the interchain interaction.

Dimensionless energy of the nearest-neighbor interchain interactions for odd k is

$$E_k = \sum_{n=2}^N U(u_{k,n} - u_{k+1,n-1}) + \sum_{n=1}^N U(u_{k+1,n} - u_{k,n}), \quad (26)$$

and for even k is

$$E_k = \sum_{n=1}^N U(u_{k,n} - u_{k+1,n}) + \sum_{n=1}^{N-1} U(u_{k+1,n+1} - u_{k,n}), \quad (27)$$

where $U(\rho)$ is the dimensionless potential of the nearest-neighbor interchain interaction.

We will consider a finite rectangular ($1 \leq n \leq N$, $1 \leq k \leq K$) with free edges, and harmonic intra- and inter-chain interaction potentials:

$$V(r) = r^2/2, \quad U(r) = r^2/4. \quad (28)$$

For the convenience of the modeling, we introduce the dimensionless quantities: temperature $\tilde{T} = T/T_0$, time $\tilde{t} = t/t_0$, and energy $E = H/E_0$, where $T_0 = \hbar^2/Ma^2k_B$, $t_0 = \hbar/k_B T_0$, and $E_0 = Ma^2/t_0^2$. Then the dimensionless Hamiltonian will have the form as

$$\mathcal{H} = \sum_{k=1}^K \sum_{n=1}^N \frac{1}{2} \dot{u}_{m,n}^2 + \sum_{k=1}^K \sum_{n=1}^{N-1} V(u_{k,n+1} - u_{k,n}) + \sum_{k=1}^K E_k, \quad (29)$$

where the dot denotes the differentiation over the dimensionless time \tilde{t} .

For the dimensionless quantities, equations of motion will take the form:

$$\ddot{u}_{kn} = -\frac{\partial \mathcal{H}}{\partial u_{kn}} - \tilde{\Gamma} \dot{u}_{kn} + \eta_{kn}, \quad k = 1, \dots, K, \quad n = 1, \dots, N \quad (30)$$

where $\tilde{\Gamma} = \Gamma t_0$ is the dimensionless friction, and the dimensionless random forces η_{kn} is the color noise with the correlation functions

$$\langle \eta_{kl}(s) \eta_{mn}(0) \rangle = 2\tilde{\Gamma} \tilde{T} \delta_{km} \delta_{ln} \int_{-\infty}^{+\infty} p(\tilde{\omega}, \tilde{T}) \exp(-i\tilde{\omega}s) \frac{d\tilde{\omega}}{2\pi}, \quad (31)$$

and dimensionless power spectral density

$$p(\tilde{\omega}, \tilde{T}) = \frac{1}{2} (\tilde{\omega}/\tilde{T}) + \frac{\tilde{\omega}/\tilde{T}}{\exp(\tilde{\omega}/\tilde{T}) - 1}, \quad (32)$$

where $\tilde{\omega} = \omega t_0$ is the dimensionless frequency. In the following we will deal only with the dimensionless quantities.

Phonons do not interact in the system with harmonic interparticle potential. Therefore the zero-point oscillations will not affect the thermal transport along the nanoribbon and can be not taken into the account. In the latter case we can consider the dimensionless random forces with the power spectra, given by $\langle \eta_{kn} \eta_{lm} \rangle_{\tilde{\omega}} = 2\tilde{\Gamma} \tilde{T} \langle S_{1kn} S_{1lm} \rangle_{\tilde{\omega}}$, cf. Eq. (20). Random forces in eq. (30) $\eta_{kn}(\tilde{t}) = \eta_{kn}(\tau/\tilde{T}) = \tilde{T} \sqrt{2\tilde{\Gamma}} S_{1kn}(\tau)$.

Within this approach, we will describe the temperature dependence of the nanoribbon thermal conductivity $\kappa(T)$. We embed the left end of the ribbon $N_e = 100$ in the thermostat with temperature $T_+ = 1.1T$, while the right end embed in the thermostat with temperature

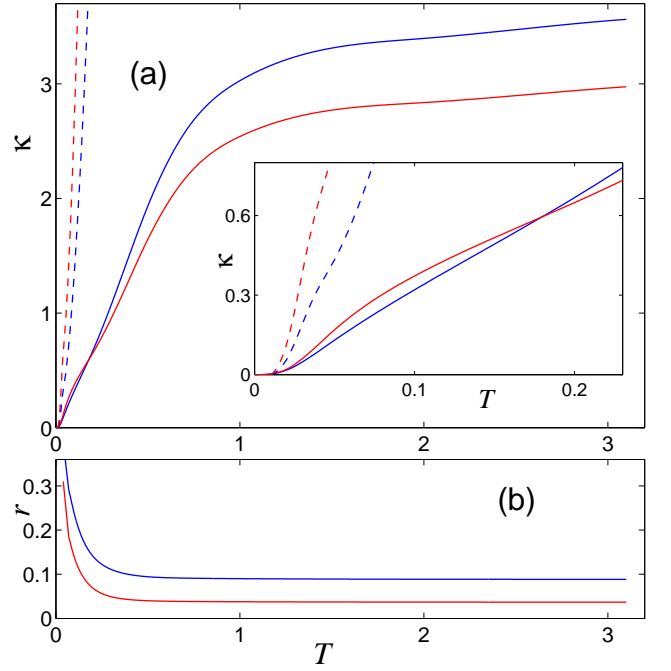


FIG. 11: (a) Thermal conductivity κ of rough-edge ribbon (ribbon width $K = 12$, rough edges widths $K_1 = 4$, atomic density of rough edges $d = 0.95$) versus temperature T for ribbon length $N = 400$ (blue line) and $N = 600$ (red line). Dashed lines give the dependencies for ideal ribbons (with atomic density of edges $d = 1$). (b) Factor of thermal conductivity suppression by rough edges r versus temperature for ribbon length $N = 400$ (blue line) and $N = 600$ (red line).

$T_- = 0.9T$. In this case the dynamics of the atoms with numbers $n = 1, \dots, N_e$ is described by Langevin equations (30) with temperature $T = T_+$, the atoms with numbers $n = N - N_e + 1, \dots, N$ are described by these equations with temperature $T = T_-$, while the atoms in the central part of the nanoribbon, with numbers $n = N_e + 1, \dots, N - N_e$, are described by the frictionless equations, Eqs. (30) with $\tilde{\Gamma} = 0$ and $\eta_{kn} \equiv 0$. We take the relaxation time $t_r = 100$, at which the edge effects at the interfaces between the ribbon and the thermostats are not essential. We integrate the equations of motion to find the stationary energy flux J along the ribbon. Then the dimensionless thermal conductivity of the finite-length ribbon can be found as

$$\kappa(N, T) = (N - 2N_e)J/[K(T_+ - T_-)]. \quad (33)$$

In the ribbon with ideal (atomically smooth) edges, phonons have infinite mean free path and therefore the energy flux J does not depend on the length of the central part of the ribbon $N_c = N - 2N_e$. In this case, as one can conclude from Eq. (33), the thermal conductivity increases linearly with N_c and therefore such ribbon behaves as an ideal (ballistic) thermal conductor. In the absence of anharmonicity of interatomic interactions, this conclusion is valid for any temperature.

We consider a ribbon which consists of $K = 12$ molecular chains. To model the roughness of the ribbon edges, we delete with probability $p = 1 - d$ some atoms from the chains with numbers $k = 1, \dots, K_1$ and $k = K - K_1 + 1, \dots, K$. Here K_1 is a width of the rough edges and $0 \leq d \leq 1$ is their atomic density. We take in the following $K_1 = 4$ and $d = 0.95$. We computed the thermal conductivity $\kappa(N, T)$ for $N = 400$ ($N_c = 200$) and $N = 600$ ($N_c = 400$), see Fig. 11. As one can see from this figure, at high (dimensionless) temperature the ribbon with the length $N = 600$ has lower thermal conductivity than the ribbon with length $N = 400$. This means that the ribbon behaves much like thermal insulator in which the thermal conductivity decreases with the length of the system, see also [16]. But the situation is changed for low temperature, for $T < 0.18$, when the longer ribbon has the higher thermal conductivity.

In this connection we can define the factor of thermal conductivity suppression by rough edges $r(T, N) = \kappa_1(N, T)/\kappa_0(N, T)$, where $\kappa_0(N, T)$ is thermal conductivity of a ribbon with ideal (atomically smooth) edges and length N , $\kappa_1(N, T)$ is thermal conductivity of the rough-edge ribbon with the same length and width. As one can see from Fig. 11 (b), the rough edges suppress the thermal conductivity for all temperatures, $r < 1$ for $T > 0$, but the suppression monotonously decreases with the decrease of temperature: for $T \rightarrow 0$ the thermal conductivities of the ideal- and rough-edge ribbons flatten, $r = \kappa_1(N, T)/\kappa_0(N, T) \rightarrow 1$. This means that long wave acoustic phonons are not scattered by surface roughness and therefore at low enough temperature the rough-edge quantum ribbon becomes an ideal (ballistic) thermal conductor, in which the thermal conductivity increases with the conductor length. This in turn means that at low enough temperature we approach the limit of ballistic *quantum thermal transport*, when the value of thermal conductance $G_{th} = J/\Delta T$, the ratio of the thermal flux J through the quasi-one-dimensional thermal conductor to the temperature difference $\Delta T = T_+ - T_-$, has a quantized value $\pi^2 k_B^2 T/3h$ (per each of the four massless acoustic modes of the quasi-one-dimensional waveguide), which does not depend on the material properties (and length) of the conductor, see, e.g., Refs. [14, 17, 18]. This property of low-temperature thermal transport is in drastic contrast to that in the classical high-temperature regime, in which the same quasi-one-dimensional rough-edge nanoribbon behaves as a thermal insulator, in which the thermal conductivity decreases with the insulator length, see Ref. [16].

VI. THERMAL CONDUCTIVITY OF NANORIBBON WITH PERIODIC INTERATOMIC POTENTIALS

In order to demonstrate the characteristic temperature dependence of thermal conductivity of quantum low-dimensional system with strongly nonlinear interatomic

interactions, we consider a ribbon with ideal (atomically smooth) edges and periodic interatomic potentials:

$$V(r) = \epsilon_1[1 - \cos(r)], \quad U(r) = \epsilon_2[1 - \cos(r)]. \quad (34)$$

In the following we will consider $\epsilon_1 = 1$, $\epsilon_2 = 0.5$, when for small relative displacements of the nearest-neighbor atoms r the potentials (34) will coincide with the harmonic potentials given by Eq. (28). With such periodic interatomic potentials, the ribbon becomes a system of coupled rotators.

A chain of coupled rotators presents a unique translationally-invariant one-dimensional system with a finite thermal conductivity [19, 20]. In such system rotobreathers can be excited, which cause strong *momentum-nonconserving* scattering of phonons and result in finite thermal conductivity of the translational-invariant system. The density of rotobreathers increases with temperature and correspondingly the phonon mean free path decreases. In the classical description, this causes the monotonous decrease of thermal conductivity κ with the increase of temperature: $\kappa \rightarrow 0$ for $T \rightarrow \infty$. In the opposite limit $T \rightarrow 0$, the phonon mean free path monotonously increases and therefore the thermal conductivity diverges: $\kappa \rightarrow \infty$ for $T \rightarrow 0$.

We consider a ribbon with a width $K = 2$ and length $N = 800$. We embed the ribbon ends of the length $N_e = 300$ each into Langevin thermostats with the color noise with temperature $T_+ = 1.1T$ for the left edge and temperature $T_- = 0.9T$ for the right one. For the relaxation time, we take $t_r = 100$. Integration of Eqs. (30) for $n = 1, \dots, N_e$ and $n = N - N_e + 1, \dots, N$, and frictionless equations, Eqs. (30) with $\tilde{\Gamma} = 0$ and η_{kn} , for $n = N_e + 1, \dots, N - N_e$, allows us to find an average energy flux along the ribbon J . With the use of Eq. (33), we then obtain the thermal conductivity of the finite-length nanoribbon.

Results of numerical modeling are presented in Fig. 12. As one can see from the temperature dependence of the nanoribbon specific heat, Fig. 12 (a), within the semi-quantum description the anharmonicity of atomic dynamics starts to show up for $T > 0.5$. Just at this temperature specific heat of the ribbon with the nonlinear interatomic potentials (34) starts to deviate from the specific heat of the ribbon with harmonic potentials (28), see Fig. 12 (a), line 2. It is worth mentioning that in the classical description the anharmonicity of lattice dynamics starts to show up for lower temperatures than that in the semi-quantum approach. This is related with the property that the anharmonicity is more pronounced in the dynamics of short wave phonons and therefore the quantum freezing out of the high frequency oscillations results in the effective decreasing of the dynamics anharmonicity (nonlinearity) at low temperature.

In the classical description, the thermal conductivity of the ribbon with nonlinear interatomic potentials (34) decreases monotonously with the increase in temperature: $\kappa \rightarrow 0$ for $T \rightarrow \infty$, see Fig. 12 (b), line 3. Within the semi-quantum description, the ribbon ther-

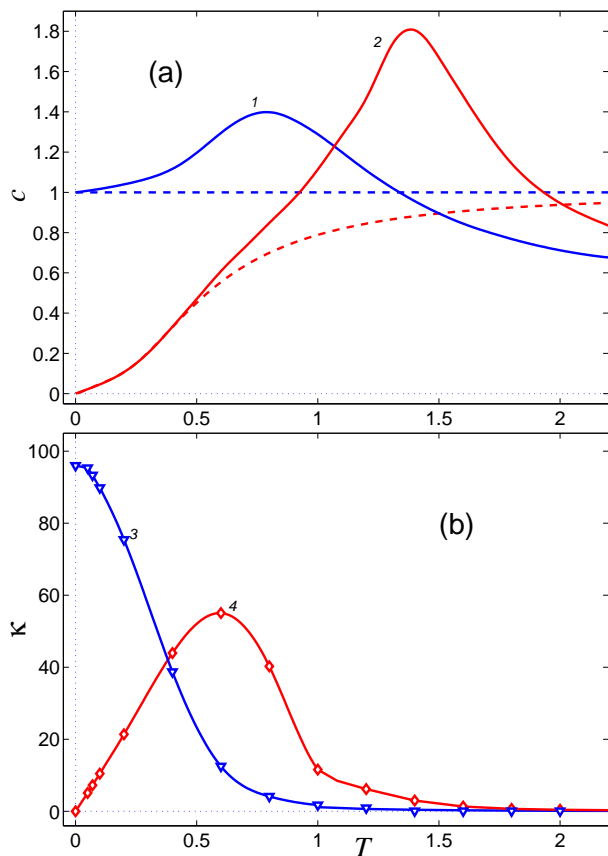


FIG. 12: (a) Specific heat c of an ideal-edge ribbon with periodic interatomic potential (34) versus temperature T , obtained within the classical (line 1) and semi-quantum (line 2) descriptions. Dashed lines show the dependencies for the ribbon with the harmonic interatomic potential (28). (b) Thermal conductivity κ versus temperature T for the ribbon with length $N = 800$ and width $K = 2$ (the length of each of the two end embedded into the thermostats with different temperatures is $N_e = 300$): lines 3 and 4 give the results obtained within the classical and semi-quantum descriptions, respectively.

mal conductivity reaches its maximal value at $T = 0.6$. For the lower and higher temperatures, the thermal conductivity decreases, $\kappa \rightarrow 0$ for $T \rightarrow 0$ and $\kappa \rightarrow 0$ for $T \rightarrow \infty$, see Fig. 12 (b), line 4. For the low temperature $T < 0.5$, system dynamics becomes almost linear when phonons propagate along the ribbon almost ballistically and the decrease of thermal conductivity is related with the quantum decrease of specific heat. For temperatures $T > 0.4$, the semi-quantum description gives higher value for the thermal conductivity than that

within the classical description. This is also related with the quantum freezing out of the high-frequency oscillations, which results in the decrease of the mean frequency of thermal phonons and correspondingly in the increase of phonon mean free path and phonon thermal conductivity. Therefore for $T > 0.4$ the effect of the increase of phonon mean free path exceeds the effect of the decrease of low temperature specific heat. At high temperatures, when phonons can be described with the classical statistics, the thermal conductivities given by the classical and semi-quantum descriptions merge, but the conductivity given by the semi-quantum description is always higher because of higher phonon mean free path under the equal, classical and semi-quantum, specific heats. The temperature dependence of thermal conductivity, given by line 4 in Fig. 12 (b), reminds the known temperature dependence of thermal conductivity in insulators, when the temperature of maximal thermal conductivity separates the low-temperature boundary-scattering regime from the high-temperature anharmonic Umklapp-scattering regime, see, e.g., Refs. [12, 13, 21, 22]. Figure 12 (b) presents one of the main results of this work.

VII. CONCLUSIONS

We present a detailed description of the semi-quantum approach to the molecular dynamics simulation of stochastic dynamics of a system of interacting particles. Within this approach, the dynamics of the system is described with the use of classical Newtonian equations of motion in which the quantum effects are introduced through the specific power spectral density of the noise (the color noise). The latter describes the interaction of the molecular system with the thermostat. We apply this approach to the simulation of specific heat and heat transport in different low-dimensional nanostructures. Within this approach, we simulate specific heat and heat transport in carbon nanotubes, as well as the thermal transport in a molecular nanoribbon with rough edges and in a nanoribbon with strongly anharmonic periodic interatomic potential. We show that the rough edges and quantum statistics of phonons change drastically the thermal conductivity of the rough-edge nanoribbon in comparison with the classical-dynamics nanoribbon with ideal (atomically smooth) edges. We show how the combination of strong nonlinearity of the interatomic potentials with quantum statistics of phonons changes the low-temperature thermal conductivity of the nanoribbon with periodic interatomic potentials.

- [1] L.D. Landau and E.M. Lifshitz. *Statistical Physics, Part 1* (Pergamon Press, Oxford, 1980).
 [2] J.-S. Wang. Quantum Thermal Transport from Classical Molecular Dynamics. *Phys. Rev. Lett.* **99**, 160601 (2007).

- [3] D. Donadio and G. Galli. Thermal Conductivity of Isolated and Interacting Carbon Nanotubes: Comparing Results from Molecular Dynamics and the Boltzmann Transport Equation. *Phys. Rev. Lett.* **99**, 255502 (2007);

- ibid.* **103**, 255502(E) (2009).
- [4] E. M. Heatwole and O. V. Prezhdo. Second-Order Langevin Equation in Quantized Hamilton Dynamics. *Journal of the Physical Society of Japan* **77**, 044001 (2008).
- [5] S. Buyukdagli, A. V. Savin and B. Hu. Computation of the temperature dependence of the heat capacity of complex molecular systems using random color noise. *Phys. Rev. E* **78**, 066702 (2008).
- [6] M. Ceriotti, G. Bussi and M. Parrinello. Nuclear Quantum Effects in Solids Using a Colored-Noise Thermostat. *Phys. Rev. Lett.* **103**, 030603 (2009).
- [7] H. Dammak, Y. Chalopin, M. Laroche, M. Hayoun and J.-J. Greffet. Quantum Thermal Bath for Molecular Dynamics Simulation. *Phys. Rev. Lett.* **103**, 190601 (2009).
- [8] J.-S. Wang, X. Ni and J.-W. Jiang. Molecular dynamics with quantum heat baths: Application to nanoribbons and nanotubes. *Phys. Rev. B* **80**, 224302 (2009).
- [9] H. B. Callen and T. A. Welton. Irreversibility and Generalized Noise. *Phys. Rev.* **83**, 34 (1951).
- [10] A. A. Maradudin, T. Michel, A. R. McGurn, E. R. Méndez. Enhanced Backscattering of Light from a Random Grating. *Annals of Physics* **203**, 255-307 (1990).
- [11] A. V. Savin, B. Hu and Y. S. Kivshar. Thermal conductivity of single-walled carbon nanotubes. *Phys. Rev. B* **80**, 195423 (2009).
- [12] R. Peierls, *Quantum Theory of Solids* (Clarendon Press, Oxford, 1955).
- [13] J. M. Ziman, *Electrons and Phonons* (Oxford University Press, Oxford, 1960).
- [14] R. Maynard and E. Akkermans. Thermal conductance and giant fluctuations in one-dimensional disordered systems, *Phys. Rev. B* **32**, 5440 (1985).
- [15] Yu. A. Kosevich. Multichannel propagation and scattering of phonons and photons in low-dimension nanostructures. *Phys-Usp.* **51**, 848 (2008).
- [16] Yu. A. Kosevich and A. V. Savin. Reduction of phonon thermal conductivity in nanowires and nanoribbons with dynamically rough surfaces and edges. *Europhys. Lett.* **88**, 14002 (2009).
- [17] L. G. Rego and G. Kirczenow. Quantized thermal conductance of dielectric quantum wires. *Phys. Rev. Lett.* **81**, 232 (1998).
- [18] K. Schwab, E. A. Henriksen, J. M. Worlock, and M. L. Roukes. Measurement of the quantum of thermal conductance. *Nature (London)* **404**, 974 (2000).
- [19] C. Giardina, R. Livi, A. Politi, and M. Vassalli. Finite thermal conductivity in 1D lattices. *Phys. Rev. Lett.* **84**, 2144 (2000).
- [20] O. V. Gendelman and A. V. Savin. Normal heat conductivity of the one-dimensional lattice with periodic potential of nearest-neighbor interaction. *Phys. Rev. Lett.* **84**, 2381 (2000).
- [21] T. Klitsner, J.E. VanClere, H.E. Fisher, and R.O.Pohl. Phonon radiative heat transfer and surface scattering. *Phys. Rev. B* **38**, 7576 (1988).
- [22] Y.-J. Han and P.G. Klemens, J.E. VanClere, H.E. Fisher, and R.O. Pohl. Anharmonic thermal resistivity of dielectric crystals at low temperatures. *Phys. Rev. B* **48**, 6033 (1993).